Coupled counterrotating polariton condensates in optically defined annular potentials

Alexander Dreismann[a], Peter Cristofolini[a], Ryan Balili[a], Gabriel Christmann[a], Florian Pinsker[b], Natasha G. Berloff[b,c], Zacharias Hatzopoulos[d,e], Pavlos G. Savvidis[a,d,f], and Jeremy J. Baumberg[a,1]

[a]Department of Physics, Cavendish Laboratory, University of Cambridge, Cambridge CB3 0HE, United Kingdom; [b]Department of Applied Mathematics and Theoretical Physics, University of Cambridge, Cambridge CB3 0WA, United Kingdom; [c]Skolkovo Institute of Science and Technology, Skolkovo 143025, Russian Federation; [d]Foundation for Research and Technology–Hellas, Institute of Electronic Structure and Laser, 71110 Heraklion, Crete, Greece; [e]Department of Physics, University of Crete, 71003 Heraklion, Crete, Greece; and [f]Department of Materials Science and Technology, University of Crete, 71003 Heraklion, Crete, Greece

Edited* by Lu Jeu Sham, University of California, San Diego, La Jolla, CA, and approved April 28, 2014 (received for review February 15, 2014)

Polariton condensates are macroscopic quantum states formed by half-matter half-light quasiparticles, thus connecting the phenomena of atomic Bose–Einstein condensation, superfluidity, and photon lasing. Here we report the spontaneous formation of such condensates in programmable potential landscapes generated by two concentric circles of light. The imposed geometry supports the emergence of annular states that extend up to 100 μm, yet are fully coherent and exhibit a spatial structure that remains stable for minutes at a time. These states exhibit a petal-like intensity distribution arising due to the interaction of two superfluids counterpropagating in the circular waveguide defined by the optical potential. In stark contrast to annular modes in conventional lasing systems, the resulting standing wave patterns exhibit only minimal overlap with the pump laser itself. We theoretically describe the system using a complex Ginzburg–Landau equation, which indicates why the condensate wants to rotate. Experimentally, we demonstrate the ability to precisely control the structure of the petal condensates both by carefully modifying the excitation geometry as well as perturbing the system on ultrafast timescales to reveal unexpected superfluid dynamics.

interferometer | rings | BEC | SQUID

Circular loops are a key geometry for superfluid and superconducting devices because rotation around a closed ring is coupled to the phase of a quantum wavefunction; so far, however, they have not been optically accessible, although this would enable a new class of quantum devices, particularly if room temperature condensate operation is achieved.

In lasing systems with an imposed circular symmetry, an annulus of lasing spots can sometimes form along the perimeter of the structure (1–6). Such transverse modes are often referred to as "petal states" (1) or "daisy modes" (2) and are interpreted as annular standing waves (3), whispering gallery modes (4), or coherent superpositions of Laguerre–Gauss (LG) modes with zero radial index (5, 6). Their circular symmetry makes them interesting for numerous applications such as free space communication or fiber coupling (7), and their LG-type structure suggests implementations using the orbital angular momentum of light (8), such as optical trapping (9) or quantum information processing (10). Petal states have been reported for various conventional lasing systems, including electrically and optically pumped vertical cavity surface-emitting lasers (VCSELs) (2, 4), as well as microchip (6) and rod lasers (1).

A fundamentally different type of lasing system is the polariton laser (11, 12). Polaritons are bosonic quasiparticles, resulting from the strong coupling between microcavity photons and semiconductor excitons (11–21). Their small effective mass (bestowed by their photonic component) and strong interactions (arising from their excitonic component) favor Bose-stimulated condensation into a single quantum state, called a polariton condensate (14, 15). These fully coherent light-matter waves spread over tens of microns (16) and exhibit a number of phenomena associated with superfluid He and atomic Bose–Einstein condensation, such as the formation of quantized vortices (17, 18) and superfluid propagation (19, 20); their main decay path is the escape of photons out of the cavity, resulting in the emission of coherent light. Note that unlike their weakly coupled counterparts, polariton lasers require no population inversion because their coherence stems from the stimulated scattering of quasiparticles into the condensate, not the stimulated emission of photons into the resonator mode (11).

In this work we study the spontaneous formation and characteristics of petal-shaped polariton condensates (Fig. 1)—the strong-coupling analog to the annular modes observed in conventional lasers. We show how the fragile ring-states observed previously (21) can be stabilized using carefully prepared optical confinement, resulting in fully coherent (*SI Appendix*, *SI Text 1*) and truly macroscopic quantum objects. We dynamically manipulate the latter both by changes of the pump geometry and ultrafast perturbations, revealing rich many-body physics, which is numerically modeled using a complex Ginzburg–Landau equation. We demonstrate an exceptional degree of control over the system suggesting the relevance of our findings for future applications such as all-optical polaritonic circuits (22–24) and interferometers (25). We furthermore emphasize differences to the weakly coupled case, arising as a consequence of the strong nonlinearities that govern the behavior of polaritons (26, 27) and the fundamentally distinct mechanism responsible for the buildup of coherence.

Significance

Collections of bosons can condense into superfluids, but only at extremely low temperatures and in complicated experimental setups. By creating new types of bosons that are coupled mixtures of optical and electronic states, condensates can be created on a semiconductor chip and potentially up to room temperature. One of the most useful implementations of macroscopic condensates involves forming rings, which exhibit new phenomena because the quantum wavefunctions must join up in phase; these are used for some of the most sensitive magnetometer and accelerometer devices known. We show experimentally how patterns of light shone on semiconductor chips can directly produce ring condensates of unusual stability, which can be precisely controlled by optical means.

Author contributions: A.D., P.C., G.C., Z.H., P.G.S., and J.J.B. designed research; A.D., P.C., R.B., and G.C. performed experiments; F.P. and N.G.B. performed theoretical analysis and numerical simulations; F.P. and N.G.B. contributed new analytic tools; Z.H. and P.G.S. managed design and growth of samples; A.D., P.C., R.B., G.C., F.P., N.G.B., and J.J.B. analyzed data; and A.D., P.C., R.B., G.C., F.P., N.G.B., and J.J.B. wrote the paper.

The authors declare no conflict of interest.

*This Direct Submission article had a prearranged editor.

[1]To whom correspondence should be addressed. E-mail: jjb12@cam.ac.uk.

This article contains supporting information online at www.pnas.org/lookup/suppl/doi:10.1073/pnas.1401988111/-/DCSupplemental.

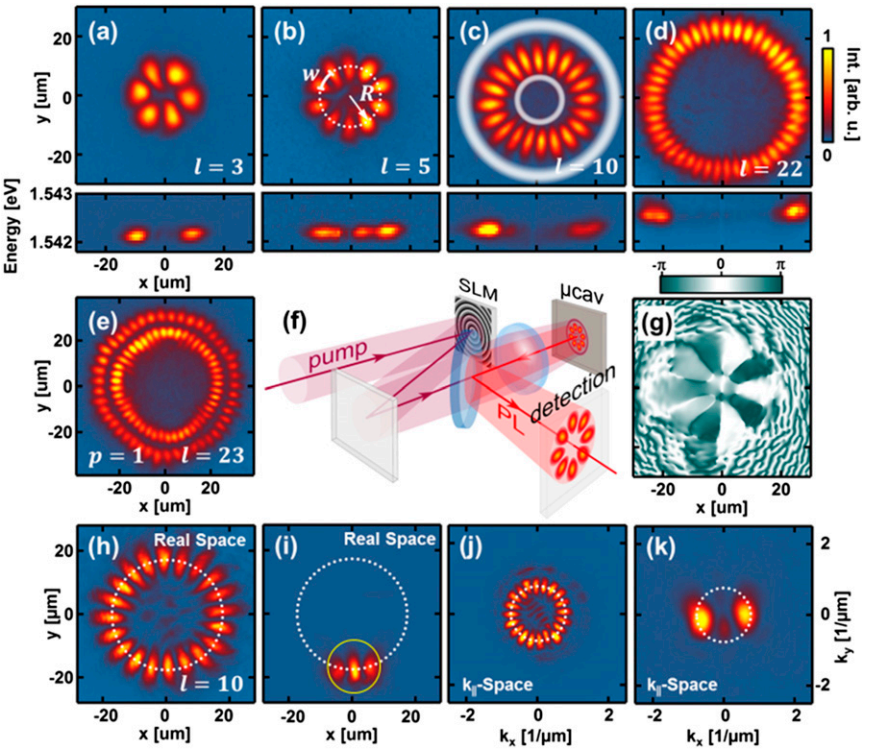

Fig. 1. Petal-shaped polariton condensates. (*A–D*) Spatial images and spectra (horizontal cut at $y = 0$) of annular states with increasing azimuthal index *l*. The shaded rings in *C* indicate the position of the pump laser. (*E*) Double-ring with radial index $p = 1$. (*F*) Schematic of the experimental setup showing the phase-shaped pump laser and the resulting polariton emission. (*G*) Phase of the condensate wavefunction in *B*, extracted following the method discussed in ref. 21. As constant reference, one of the lobes was magnified and superimposed over the whole image. (*H–K*) Real- and *k*-space images of a petal state with $l = 10$. The *k*-space image in *K* is obtained by spatially filtering the polariton emission, as shown in *I*.

Petal Condensates

Our experimental setup uses a high-resolution spatial light modulator (SLM), which allows phase-shaping of the pump laser into the desired intensity-patterns on the sample (Fig. 1*F*). Results here were obtained from a high-quality, low-disorder AlGaAs/AlAs microcavity, incorporating four sets of three GaAs quantum wells. We nonresonantly excite our sample with a single-mode continuous-wave laser, at energies ∼100 meV above the bottom of the lower polariton branch. The resulting polariton emission is detected with a CCD for imaging, a monochromator plus CCD for spectral analysis, and a streak camera for monitoring its temporal evolution. A Fourier lens and Mach–Zehnder interferometer are used to probe *k*-space distribution and first-order coherence. All measurements were performed at cryogenic temperatures and on sample locations where the cavity mode is tuned ∼7 meV below that of the exciton.

The excitation pattern used to stably generate petal-type condensates consists of two concentric circles of laser light (Fig. 1*C*, white rings), with a local intensity ratio for inner to outer circle of 1:8. The nonresonant excitation results in the formation of a cloud of hot excitons at the position of the pump, which subsequently relax in energy, couple to the cavity mode, and accumulate at the bottom of the lower polariton branch. Because of their repulsive interactions, polaritons experience a local blueshift at positions of high exciton density (16, 28); for the given pump geometry, this induces a potential landscape resembling an annular waveguide. Strikingly, the resulting polariton condensate forms in the region between the outer and the inner pump ring, thus—unlike conventional lasing systems (6, 29) and contrary to Manni et al. (21)—exhibiting only minimal overlap with the pump laser itself (Fig. 1*C*). This effect is a direct consequence of the specific properties of polaritons—namely, their strong nonlinear interactions with the hot exciton cloud and their ability to propagate over tens of micrometer distances before they decay (16, 28). The resulting petal condensates possess a well-defined energy and exhibit a characteristic annular intensity distribution (Fig. 1 *A–D*), which remains stable for >1,000-s timescales. The real space image of a ring with *n* intensity lobes translates into a reciprocal space image with an identical number of lobes, where the emission coming from a specific lobe in real space stems from polaritons with equal and opposite wave vectors around the annulus (Fig. 1 *H–K*). This observation yields the picture of two counterpropagating superfluids, analogous to superconducting loops and qubits (30, 31). Because both waves are subject to periodic boundary conditions, their superpositions always possess an even number of lobes with a well-defined phase and a phase jump of π in between lobes (Fig. 1*G*). Mathematically, these properties are consonant with a description as superpositions of two $LG_{p,\pm l}$ modes with radial index $p = 0$ and azimuthal indices $\pm l$, where the number of lobes *n* is given by $n = 2l$ (*SI Appendix, SI Text 2*).

Adjusting the diameter of the excitation pattern allows the selection of petal states with an arbitrary even number of lobes, up to a (power-limited) maximum of $n \approx 120$. However, increasing the separation between inner and outer pump rings results in the formation of higher-order ring states with radial nodes ($p > 0$) and identical *n* (Fig. 1*E*). The orientation of the nodal lines depends on the relative phase of the two counterpropagating waves; for a uniform pump, it is pinned by local disorder, as can be seen from the rotation of the condensate as we move across the sample (Movie S1), matching similar observations for the case of VCSELs (2). However, azimuthally modulating the pump intensity allows us to freely select the orientation of the petals, further demonstrating the high degree

of control possible over the system (*SI Appendix, SI Text 3*). These ring states are highly resilient to irregularities of the sample surface, maintaining their shape even in the presence of cracks and other defects (*SI Appendix, SI Text 4*).

Power Dependence

To explore the formation process of the reported ring-shaped condensates, we study the evolution of the system as the excitation power increases (Fig. 2). The latter causes a growth of the density-induced blue-shift potential V_0 at the position of the pump, accelerating polaritons away from the region of their creation and up to a final velocity $v_{max} \approx \sqrt{2V_0/m^*}$, where m^* is the polariton effective mass. For low pump powers, the excited polaritons gain only little momentum and hence cover only short distances before they decay; consequently, pump and polariton luminescence coincide (Fig. 2 *A* and *E*). However, as pump intensity and blue-shift increase, so does the momentum of the polaritons. Those traveling toward the center of the pump geometry are eventually slowed down by the potential associated with the inner ring and accumulate in the region between both rings (Fig. 2 *B* and *E*). This accumulation is further enhanced by stimulated scattering of polaritons directly from the pump, as can be seen from the nonlinear increase of polariton emission from the region between the laser rings even below threshold (green line in Fig. 2*D*). At sufficiently high powers, the corresponding polariton population reaches the critical density for condensation and a petal-state forms (Fig. 2*C*), with the polariton wave vector k_c pointing around the annulus. The formation of the condensate is accompanied by a strong nonlinear increase of emission intensity, and the number of polaritons outside the pump ring decreases (Fig. 2 *D* and *E*). The latter effect suggests that the condensate now efficiently harvests almost all polaritons created at the pump due to stimulated scattering, as reported for optically confined condensates previously (32). Increasing the excitation power beyond the condensation threshold P_{thr} quickly leads to the breakdown of the single ring-state, which, unlike in the work of Manni et al. (21), is only observed within a narrow power range up to 1.3 P_{thr}. We attribute this observation to the repulsive nature of polariton–polariton interactions, which blue-shift the condensate energy with increasing density and eventually screen the influence of the inner pump ring, allowing a superposition of higher-order states to fill up the whole excitation geometry (*SI Appendix, SI Text 5*).

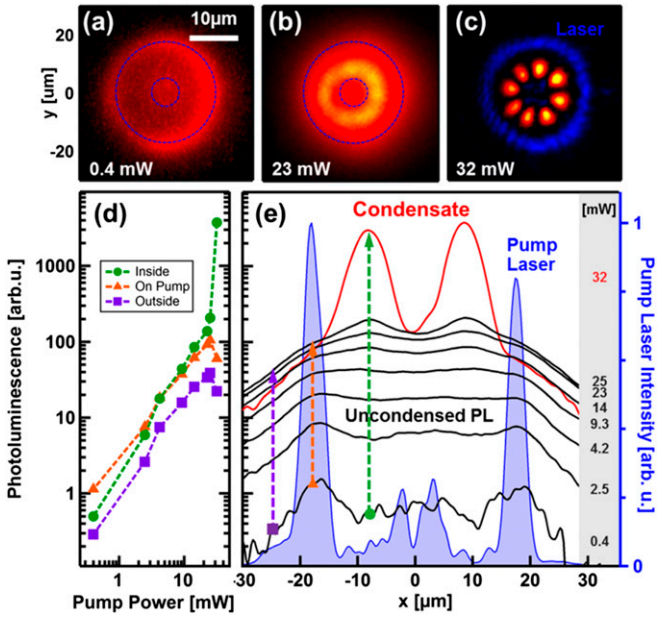

Fig. 2. Sample luminescence with increasing excitation power. (*A*–*C*) Spatial image of the polariton emission with increasing pumping power. Dashed blue line indicates the position of the laser as shown in *C*. (*D* and *E*) Power dependence of the intensity distribution along a central horizontal cut.

Mode Selection

We next use the flexibility of our setup to systematically vary the pump geometry and study the mode selection mechanism linking a specific excitation pattern to the resulting petal state. As the diameter of the pump ring is gradually increased, the number of lobes n is found to grow as $n \propto r_c^2$, where r_c denotes the radius of the condensate ring (Fig. 3*A*, green points). Note that in all cases the condensate forms in the region between the two pump rings.

A qualitative explanation for this observation can be found by considering that condensation will initially occur at the point of highest polariton density. Just below threshold, this location corresponds to the doughnut-shaped region between the two pump rings, as can be seen from the distribution of polariton emission in Fig. 2*B*. The optimum overlap between this low-energy polariton reservoir with radius r_{res} and the condensate pattern is achieved for LG_{0l} states of identical radius, i.e., $r_c = r_{res}$ (5, 6). Consequently, these states possess the lowest condensation threshold and first start oscillating as the pumping increases. Because this argument holds equally for the energetically degenerate left- and right-handed $LG_{\pm l}$ modes, both are excited simultaneously, resulting in the observed standing wave patterns. The radius of maximum intensity for a superposition of $LG_{0\pm l}$ modes lies at $r_c = w\sqrt{l/2}$, where w denotes the width of the cavity's fundamental mode (*SI Appendix, SI Text 2*). Taking into account that the number of lobes n is given by $n = 2l$, we arrive at the relation $n = [2/w]^2 r_c^2$, which reproduces the experimental data for $w \approx 9.3$ μm (Fig. 3*A*, green line).

Theoretical Description

To theoretically approach the observed phenomena we use a complex Ginzburg–Landau (cGL)-type equation (33, 34) incorporating energy relaxation (35) and a stationary reservoir:

$$i\partial_t\psi = (1 - i\eta)\frac{H}{\hbar}\psi$$

$$\frac{H}{\hbar} = \left[-\frac{\hbar\nabla^2}{2m} + V(\boldsymbol{x},t) + \frac{i}{2}(\delta_R N(\boldsymbol{x},t) - \gamma_C)\right]. \qquad [1]$$

Here, ψ represents the order parameter of the condensate, η the rate of energy relaxation, and m the effective mass of polaritons on the lower branch of the dispersion curve; $\delta_R N/2$ and γ_C are the condensate gain and loss rates, respectively; and $V(\boldsymbol{x},t) = g_R N + g_C|\psi|^2 + V_{dis}$ denotes the potential landscape experienced by the condensate, which arises due to interactions with the reservoir ($g_R N$), polariton–polariton interactions ($g_C|\psi|^2$) and energy fluctuations due to sample disorder (V_{dis}). The radially symmetric pumping profile $P(r)$ is chosen to reproduce the experimental double-ring excitation geometry (*SI Appendix, SI Text 6*), giving rise to a reservoir density distribution following $\partial_t N = -(\gamma_R + \beta|\psi|^2)N + P$, where γ_R represents the reservoir decay and β the condensate reservoir scattering rate. Because the relaxation of the reservoir is much faster than the decay of the condensate ($\gamma_R \gg \gamma_C$) (34), the reservoir dynamics can be approximated by the stationary value $N \approx P/(\gamma_R + \beta|\psi|^2) \approx P/\gamma_R + (P\beta/\gamma_R^2)|\psi|^2$, where in the second step the magnitude of ψ was assumed to be small.

Numerical solutions of Eq. **1** for the parameters given in *Materials and Methods* are presented in Fig. 3. The simulated condensate density and corresponding phase (Fig. 3 *B* and *C*) are

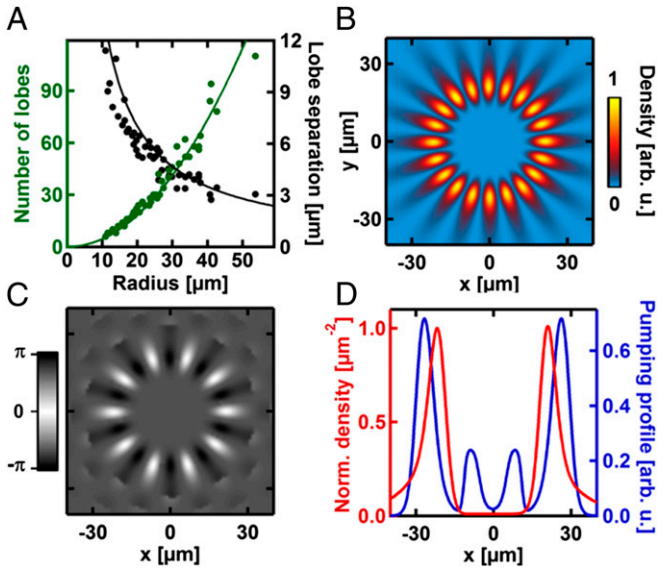

Fig. 3. (*A*) Measured number of lobes n (green points) and spatial separation between lobes (black points) as a function of condensate radius r_c. Fits are obtained from simulations of the cGL equation for different pump radii (*SI Appendix, SI Text 6*) or the analytic expression for the density maximum of LG modes (*SI Appendix*, Eq. **S4**). (*B*) Simulated spatial density of a petal condensate with $n = 20$ lobes and (*C*) corresponding phase. (*D*) Horizontal cut of *B*, indicating the relative position of the condensate and the pumping profile.

obtained for a pumping profile matching that of Fig. 1*C*. The simulation clearly reproduces the observed petal structure with $n = 20$ lobes. Note that energy relaxation and disorder prove critical to stabilize the angular orientation of the calculated petal modes (*SI Appendix*, *SI Text 6*). The maxima of condensate and reservoir are spatially separated (Fig. 3*D*) in accordance with the experiment (Fig. 2*E*), although their separation is less pronounced in the simulation (Fig. 2*E*). We attribute this deviation to the simplicity of our model, which does not incorporate the propagation of uncondensed polaritons. Gradually increasing the radius of the simulated pumping profile results in the formation of states with a higher (even) number of lobes. The relation between condensate radius and lobe number agrees precisely with the experimental data (Fig. 3*A*, green and black lines, and *SI Appendix*, *SI Text 6*). An analytic estimation for the observed relation is provided in *SI Appendix*, *SI Text 7*.

Note that the formation of lobes corresponds to excitations of the system's ground state. In the linear picture the latter are associated with the larger in-plane wave vectors of higher-order LG modes, whereas from the viewpoint of a (nonlinear) complex Ginzburg–Landau equation, the π phase-jumps observed between adjacent lobes and the vanishing condensate density can be interpreted as a signature of dark solitons or solitary waves. However, the standing wave pattern appears in simulations even if the real nonlinearity is set to zero ($g_C = 0$). The weak nonlinearity slightly modifies the density profile, but does not change the number or position of the lobes. Though this implies that the formation mechanism of the petal structure can be understood in terms of linear physics, the condensate itself and each of its lobes still represent a highly nonlinear system due to polariton–polariton interactions. Arrays of the lobes represent excitations of the condensate ground state and can arise due to the interaction of counterpropagating superfluids in an effective 1D setting (36, 37). We assume that the reported ring condensates occupy excited states instead of their ground states to maintain energy conservation: polaritons generated in the blue-shifted pumping regions that scatter into the condensate lack an efficient mechanism for energy relaxation (28), as evidenced by the fact that both possess the same energy (*SI Appendix*, *SI Text 8*). Because the blue-shift at the position of the condensate is much smaller than that at the pump, the condensate must form in an excited state, translating into a transverse wave vector $k_c > 0$ (linear picture) or the formation of an array of dark solitary waves (nonlinear picture).

Increasing the radius of the pump rings results in the formation of states with a higher number of lobes, corresponding to higher condensate energies (*SI Appendix*, *SI Text 9*). Qualitatively, one can associate this increasing n with an accelerated rotation of the two counterpropagating condensates. A related phenomenon was studied in ref. 33, where the authors show that inhomogeneous pumping of large-area trapped condensates can spontaneously induce condensate rotation and the formation of vortex lattices. Assuming the annular waveguide forms a harmonic trap with level spacing $\hbar\omega$, the stable rotation speed is $\Omega = n_V/\tilde{r}^2 = 1$, where $\tilde{r} = r/\sqrt{\hbar/m\omega}$; n_V represents the number of vortices in the lattice and was shown to grow quadratically with the radius of the pump. However, we note that this intuitive explanation does not include the presence of two counterpropagating condensates, and that given the 1D geometry here, vortex pairs are not seen (37) but instead a standing wave with the full condensate density depletions.

Condensate Dynamics

To explore the time dynamics of the system, we nonresonantly perturb the continuously-pumped petal condensate with a 150-fs pulsed laser, which is focused on the side of the ring (Fig. 4*A*, *Inset*). Fig. 4*A* shows a cylinder projection of the polariton emission around the condensate ring at different times t, as reconstructed from a full set of tomographic streak camera measurements. Before it is perturbed ($t < 0$ ps), the condensate forms a stable petal state with $n = 22$ lobes. The initial effect of the perturbing pulse P at $t = 0$ ps is a strong reduction of the overall polariton emission after ~2 ps (Fig. 4 *A* and *B*). We attribute this behavior to photons that are rapidly generated by the

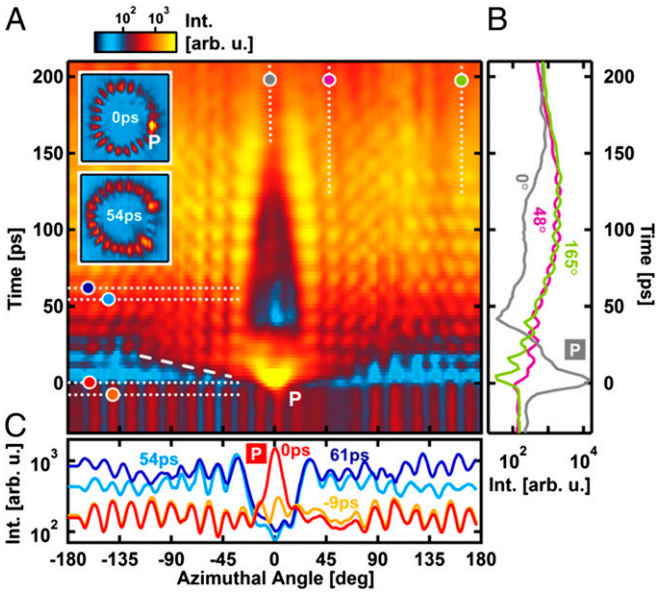

Fig. 4. Time dynamics of a perturbed petal condensate. (*A*) Cylinder projection of the polariton emission around the condensate annulus at different times t. The perturbing pulse P arrives at $t = 0$ ps. (*Insets*) Spatial images of the condensate ring at $t = 0$ ps and $t = 54$ ps. Dotted lines indicate the position of space cuts depicted in *B* and time cuts depicted in *C*. Dashed line is a guide to the eye. (*Insets*) Spatial images at different times.

laser pulse and subsequently propagate ballistically across the cavity, where they extract gain from the exciton reservoir due to stimulated emission into the wave-guided mode. The additional exciton population locally introduced by the laser pulse creates a localized blue-shift potential barrier, analogous to the weak links forming Josephson junctions in superconducting loops and superconducting quantum interference devices. The potential barrier breaks up the ring state by pushing apart its lobes while transiently reducing their number, corresponding to a reduction of the respective vorticity of each counter-propagating wave. Note that the modified potential landscape at this point no longer imposes periodic boundary conditions on the system, thus allowing the formation of states with an odd number of lobes as well. The additional gain provided by the laser pulse creates an imbalance of the polariton density around the ring (Fig. 4*B*, green and pink lines). The high density of polaritons formed on either side of the disturbance propagates along the annulus at a velocity $v \approx 1.3$ μm/ps (dashed line in Fig. 4*A*), matching that expected for polariton wave packets oscillating in a harmonic potential (32). As a consequence, density oscillations with a period of $T \approx 14$ ps are observed when the lobes are perturbed sideways by the impulse (Fig. 4 *B* and *C*). As the exciton reservoir generated by the laser pulse decays and further feeds the condensate, the overall polariton emission increases above its initial value due to the additional gain provided (Fig. 4 *A* and *B*). The reduction of the corresponding potential barrier at the same time allows the convergence of the separated lobes and finally the reformation of the petal state after $t > 400$ ps. Simulations confirm that this behavior is characteristic of the cGL nonlinear quantum dynamics (Movie S2).

Summary and Conclusion

We have studied the properties of exciton–polariton condensates in optically imposed annular potentials. The pumping geometry supports the formation of quantum states that extend up to 100 μm, are highly resilient to defects and sample disorder, and remain stable for minutes at a time. The observed phenomena are reproduced by simulations of a cGL-type equation. The spatial separation of pump reservoir and condensate minimizes dephasing and other perturbations due to interactions with hot excitons (38), thus making this excitation geometry highly advantageous for stable macroscopic quantum devices operating at ultralow thresholds.

Exploitation of such states on semiconductor chips is analogous to those of superconducting weak-link devices. Because the pure $LG_{0,\pm l}$ modes carry a net orbital angular momentum associated with a helically propagating phase and exhibit a vortex in their center, lifting the degeneracy between the counter propagating modes (e.g., with magnetic fields) can result in a pure rotating condensate with giant stable vortex core. The ability to sculpt the polariton potentials into arbitrary shapes (*SI Appendix*, *SI Text 10*) opens up new explorations of condensate superfluid flow in a wide variety of topologies.

Materials and Methods

The sample consists of a $5\lambda/2$ AlGaAs/AlAs microcavity, with a quality factor exceeding $Q > 16{,}000$, corresponding to cavity photon lifetimes $\tau > 7$ ps. Four sets of three GaAs quantum wells are placed at the antinodes of the cavity optical field, with an exciton–photon Rabi splitting of 9 meV. All reported experiments were performed at sample positions where the cavity mode is detuned 7 meV below the exciton energy.

The system is pumped with a $\lambda = 755$-nm single-mode continuous wave Ti:Sapphire laser, which is projected through a 4× telescope and a 50× high-N.A. microscope objective acting as a Fourier lens. The resulting polariton emission of ∼800 nm is collected with the same microscope objective and separated from the laser radiation by means of a tunable Bragg filter; it is detected by a Si CCD for imaging, a 0.55-m monochromator with a nitrogen-cooled CCD for spectral analysis and a streak camera (time resolution 2.5 ps) for monitoring the temporal evolution. A Fourier lens and a Mach–Zehnder interferometer were used to probe its *k*-space distribution and first-order coherence.

The parameters used in the simulation were chosen in agreement with refs. 21, 35, and 39, where energy relaxation rate $\eta = 0.02$, reservoir decay rate $\gamma_R = 10\ \text{ps}^{-1}$, condensate decay rate $\gamma_C = 0.556\ \text{ps}^{-1}$, reservoir interaction constant $g_R = 0.072\ \mu\text{m}^2 \cdot \text{ps}^{-1}$, self-interaction constant $g_C = 0.002\ \mu\text{m}^2 \cdot \text{ps}^{-1}$, factor of condensate gain rate $\delta_C = 0.06\ \mu\text{m}^2 \cdot \text{ps}^{-1}$, and condensate reservoir scattering rate $\beta = 0.05\ \mu\text{m}^2 \cdot \text{ps}^{-1}$. The effective mass of the lower polariton branch was measured as $m = 4.7 \cdot 10^{-35}$ kg.

ACKNOWLEDGMENTS. We acknowledge funding from Engineering and Physical Sciences Research Council Grant EP/G060649/1, European Union Grant INDEX 289968, Spanish Ministry of Economic Competitiveness Grant MAT2008-01555, Leverhulme Grant VP1-2013-011, Greek General Secretariat of Research and Technology ARISTEIA Programs Irakleitos II and Apollo, and the Skolkovo Foundation.

1. Senatsky Y, et al. (2012) Laguerre–Gaussian modes selection in diode-pumped solid-state lasers. *Opt Rev* 19(4):201–221.
2. Pereira SF, Willemsen MB, van Exter MP, Woerdman JP (1998) Pinning of daisy modes in optically pumped vertical-cavity surface-emitting lasers. *Appl Phys Lett* 73(16): 2239–2241.
3. Schulz-Ruhtenberg M, Tanguy Y, Jäger R, Ackemann T (2009) Length scales and polarization properties of annular standing waves in circular broad-area vertical-cavity surface-emitting lasers. *Appl Phys B* 97(2):397–403.
4. Deng Q, Deng H, Deppe DG (1997) Radiation fields from whispering-gallery modes of oxide-confined vertical-cavity surface-emitting lasers. *Opt Lett* 22(7):463–465.
5. Naidoo D, Aït-Ameur K, Brunel M, Forbes A (2012) Intra-cavity generation of superpositions of Laguerre–Gaussian beams. *Appl Phys B* 106(3):683–690.
6. Chen YF, Lan YP, Wang SC (2001) Generation of Laguerre–Gaussian modes in fiber-coupled laser diode end-pumped lasers. *Appl Phys B* 72(2):167–170.
7. Grabherr M, Miller M, Jäger R, Wiedenmann D, King R (2004) Commercial VCSELs reach 0.1 W cw output power. *Proc SPIE* 5364:174–182.
8. Allen L, Beijersbergen MW, Spreeuw RJC, Woerdman JP (1992) Orbital angular momentum of light and the transformation of Laguerre–Gaussian laser modes. *Phys Rev A* 45(11):8185–8189.
9. Rodrigo JA, Caravaca-Aguirre AM, Alieva T, Cristóbal G, Calvo ML (2011) Microparticle movements in optical funnels and pods. *Opt Express* 19(6):5232–5243.
10. Molina-Terriza G, Torres JP, Torner L (2007) Twisted photons. *Nat Phys* 3(5):305–310.
11. Imamoglu A, Ram RJ, Pau S, Yamamoto Y (1996) Nonequilibrium condensates and lasers without inversion: Exciton-polariton lasers. *Phys Rev A* 53(6):4250–4253.
12. Deng H, Weihs G, Snoke D, Bloch J, Yamamoto Y (2003) Polariton lasing vs. photon lasing in a semiconductor microcavity. *Proc Natl Acad Sci USA* 100(26):15318–15323.
13. Weisbuch C, Nishioka M, Ishikawa A, Arakawa Y (1992) Observation of the coupled exciton-photon mode splitting in a semiconductor quantum microcavity. *Phys Rev Lett* 69(23):3314–3317.
14. Kasprzak J, et al. (2006) Bose–Einstein condensation of exciton polaritons. *Nature* 443(7110):409–414.
15. Balili R, Hartwell V, Snoke D, Pfeiffer L, West K (2007) Bose-Einstein condensation of microcavity polaritons in a trap. *Science* 316(5827):1007–1010.
16. Wertz E, et al. (2010) Spontaneous formation and optical manipulation of extended polariton condensates. *Nat Phys* 6(11):860–864.
17. Lagoudakis KG, et al. (2008) Quantized vortices in an exciton-polariton condensate. *Nat Phys* 4(9):706–710.
18. Sanvitto D, et al. (2010) Persistent currents and quantized vortices in a polariton superfluid. *Nat Phys* 6(7):527–533.
19. Amo A, et al. (2009) Superfluidity of polaritons in semiconductor microcavities. *Nat Phys* 5(11):805–810.
20. Amo A, et al. (2009) Collective fluid dynamics of a polariton condensate in a semiconductor microcavity. *Nature* 457(7227):291–295.
21. Manni F, Lagoudakis KG, Liew TCH, André R, Deveaud-Plédran B (2011) Spontaneous pattern formation in a polariton condensate. *Phys Rev Lett* 107(10):106401.
22. Liew TCH, Kavokin AV, Shelykh IA (2008) Optical circuits based on polariton neurons in semiconductor microcavities. *Phys Rev Lett* 101(1):016402.
23. Amo A, et al. (2010) Exciton-polariton spin switches. *Nat Photonics* 4(6):361–366.
24. Gao T, et al. (2012) Polariton condensate transistor switch. *Phys Rev B* 85(23):235102.
25. Franchetti G, Berloff NG, Baumberg JJ (2012) arXiv:1210.1187.
26. Nardin G, et al. (2009) Dynamics of long-range ordering in an exciton-polariton condensate. *Phys Rev Lett* 103(25):256402.
27. Spano R, et al. (2012) Coherence properties of exciton polariton OPO condensates in one and two dimensions. *New J Phys* 14(July):075018.
28. Christmann G, et al. (2012) Polariton ring condensates and sunflower ripples in an expanding quantum liquid. *Phys Rev B* 85(23):235303.
29. Naidoo D, et al. (2011) Transverse mode selection in a monolithic microchip laser. *Opt Commun* 284(23):5475–5479.
30. Kleiner R, Koelle D, Ludwig F, Clarke J (2004) Superconducting quantum interference devices: State of the art and applications. *Proc IEEE* 92(10):1534–1548.
31. Orlando TP, et al. (1999) Superconducting persistent-current qubit. *Phys Rev B* 60(22): 15398–15413.

32. Cristofolini P, et al. (2013) Optical superfluid phase transitions and trapping of polariton condensates. *Phys Rev Lett* 110(18):186403.
33. Keeling J, Berloff NG (2008) Spontaneous rotating vortex lattices in a pumped decaying condensate. *Phys Rev Lett* 100(25):250401.
34. Wouters M, Carusotto I (2007) Excitations in a nonequilibrium Bose-Einstein condensate of exciton polaritons. *Phys Rev Lett* 99(14):140402.
35. Wouters M, Liew T, Savona V (2010) Energy-relaxation in one-dimensional polariton condensates. *Phys Rev B* 82(24):245315.
36. Scott TF, Ballagh RJ, Burnett K (1998) Formation of fundamental structures in Bose-Einstein condensates. *J Phys At Mol Opt Phys* 31(8):329–335.
37. Pinsker F, et al. (2013) Nonlinear quantum piston for the controlled generation of vortex rings and soliton trains. *Phys Rev A* 87(5):053624.
38. Askitopoulos A, et al. (2013) Polariton condensation in an optically induced two-dimensional potential. *Phys Rev B* 88(4):041308.
39. Ge L, Nersisyan A, Oztop B, Türeci HE (2013) Pattern formation and strong nonlinear interactions in exciton–polariton condensates. arXiv:1311.4847.